Study on Chip Formation in Grinding of Nickel-Based Polycrystalline Superalloy GH4169

Tao Zhu
Liaoning Petrochemical University
Ming Cai (caiming199004@126.com)
Liaoning Petrochemical University
Yadong Gong
Northeastern University
Xingjun Gao
Liaoning Petrochemical University
Ning Yu
Liaoning Petrochemical University
Xiang Li
Liaoning Petrochemical University

Research Article

Keywords: nickel-based superalloy GH4169, chip formation, finite element simulation, grinding

Posted Date: December 29th, 2021

DOI: https://doi.org/10.21203/rs.3.rs-1195267/v1

Study on chip formation in grinding of nickel-based polycrystalline superalloy GH4169

Tao Zhu [a], Ming Cai [a, *], Yadong Gong [b], Xingjun Gao [a], Ning Yu [c], Xiang Li [a]

[a] *School of Mechanical Engineering, Liaoning Petrochemical University, Fushun, 113001, China*

[b] *School of Mechanical Engineering and Automation, Northeastern University, Shenyang, 110819, China*

[c] *School of Innovation and Entrepreneurship, Liaoning Petrochemical University, Fushun, 113001, China*

* Corresponding author e-mail addresses: caiming199004@126.com (Ming Cai)

Abstract Based on the variation of the actual cutting depth during the grinding process, a 3D finite element (FE) simulation model for grinding nickel-based superalloy GH4169 with single abrasive was initially constructed. Then the morphological evolution of the grinding chips during the grinding process was studied. In addition, the effect of the single abrasive cutting depth and the grinding speed on chip morphology and segmentation frequency was investigated. Finally, experimental results with the same test parameters verify the finite element simulation results. The results showed that in the experimental grinding speed range, the sawtooth lamellar chip with the free surface being serrated and the contact surface being smooth due to the extrusion of the abrasive is easy to produce when grinding nickel-based superalloy GH4169. As the grinding speed increases, the chip morphology changes from a unitary lamellar chip to a continuous serrated chip, developing into a continuous ribbon chip. The chip segmentation frequency is mainly determined by grinding depth and grinding speed. To be specific, the smaller the grinding depth and the greater the grinding speed, the greater the chip formation frequency.

Keywords nickel-based superalloy GH4169; chip formation; finite element simulation; grinding

1 Introduction

Nickel-based superalloys can serve in high-temperature (600~1100°C) environments and can be subjected to various high-temperature complex cyclic stresses, with excellent high-temperature strength, creep resistance and corrosion resistance, and have been widely used in aero-engine turbine blades, turbine discs and other core components. However, the excellent physical properties of nickel-based superalloys can lead to various difficulties, such as low machining efficiency, poor surface quality and high machining costs. A great number of tests and investigations on nickel-based superalloys have been conducted by researchers, with positive results. They intend to enhance the surface quality of workpieces, improve the machining properties of difficult-to-machine materials and increase machining efficiency.

Li et al. [1] conducted ultrasonic vibration-assisted grinding of Inconel 718 with electroplated CBN grinding wheels. Gong et al. [2] developed a model for predicting the normal and tangential forces of a nickel-based single crystal superalloy. The authors investigated the impact of grinding parameters on grinding forces, surfaces, and subsurfaces. Zhou et al. [3] analyzed the effects of grinding speed, wheel feed rate and cutting depth on the roughness of nickel-based superalloy DD98 by response surface methodology. Gu et al. [4] discovered that the

microcrystalline alumina grinding wheel outperformed the brown corundum grinding wheel in terms of grinding force, G-ratio, and specific grinding energy while grinding nickel-based single crystal superalloy DD6. Miao et al. [5] used alumina grinding wheels to perform trials on several nickel-based superalloys and discovered that the grinding wheel mostly suffered abrasive wear while grinding DZ408, K403, and GH4169, but primarily encountered abrasive clog when grinding DD6. Dai et al. [6-7] investigated the effect of diamond grain cutting edge morphology and grinding speed on the machining performance of Inconel 718. Cai et al. [8-9] evaluated the machining process parameters and performed orthogonal tests on the grinding surface quality of the nickel-based single crystal superalloy DD5. Ding et al. [10] effectively predicted the grinding surface topography by reconstructing the measured surface topography of CBN grinding wheels. Ruzzi et al. [11] evaluated the effect of several grinding parameters on the surface profile of the Inconel 718.

The essence of grinding is the removal of workpiece material through the synergy between the cutting edges of tens of thousands of tiny abrasive grains on the grinding wheel [12]. Because of the large number of abrasives involved, it is more difficult to study the chip formation pattern of nickel-based superalloys and it is more difficult to carry out a quantitative analysis. By simplifying the number of abrasives and using single abrasive grinding to study chip formation, the variation in the chip formation mechanism can be observed to a large extent for different grinding parameters. The validity of this simplified approach has also been confirmed by international researchers. To be specific, Öpöz and Chen [13-15] looked into the material removal process of single abrasive grinding and discovered that single-edged abrasive is more efficiently removed, while multi-edged abrasive is more likely to plough. Zhao and Chen et al. [16-17] measured the grinding forces, the maximum undeformed cutting thickness and the grinding morphology at different speeds. Tian et al. [18] explored the influence of grinding speed on the removal of nickel-based superalloy GH4169 material by the single abrasive test method and studied the critical chip-forming thickness of chip formation. Feng et al. [19] investigated the formation of scratches, chips and grinding forces during single grain grinding. The influence of grinding parameters on the ground surface of Inconel 625 was analyzed by Ruzzi et al. [20]. They discovered that Inconel 625 is particularly vulnerable to work hardening during the grinding process, with grinding speed having the most significant impact. Li et al. [21] developed a grinding force model based on the single abrasive cutting process and verified the accuracy of the model by orthogonal grinding tests. Denkena et al. [22] proposed a new method to experimentally analyze the mechanism of chip formation during grinding.

The finite element simulation models with a single abrasive were established by scholars to observe more intuitively the changes in the chip formation mechanism and its formation mechanism during grinding. Brinksmeier et al. [23] presented an overview of modeling and simulation. Chen et al. [24] established a model for the thermal coupling between the grinding abrasive and the workpiece to study the residual stresses induced during ultra-high-speed grinding and analyze the effect of different conditions on the residual stress distribution using mathematical statistics. Esmaeili et al. [25] established a single abrasive simulation model and found that under adiabatic conditions, an increase in cutting speed and a decrease in the cutting edge front angle resulted in discontinuous chip generation. Fu et al. [26] analyzed the effects of grinding speed and cutting thickness on the grinding force and stress distribution. Zhang and Choi [27] observed that thermal shear zones were not only generated at the chip root but also on the free surface of the abrasive chips by developing an orthogonal experimental simulation model for titanium alloys. Dai et al. [28] determined the critical chip formation velocity of the nickel-based superalloy Inconel 718 by building single abrasive simulation model and found that the critical

chip formation velocity was 150 m/s. Zhou et al. [29] determined the critical chip-forming thickness and critical tough-brittle transition thickness of SiC single abrasive grains by building a simulation model.

It should be emphasized that, despite the fact that a considerable number of research on single abrasives have been conducted in recent years, the finite element simulation models with single abrasive is mainly focused on the modeling simulation of a two-dimensional model, where the grinding depth of the model is constant and the actual path changes are not considered. In this study, a three-dimensional simulation model was founded according to the actual cutting thickness of the single abrasive during the grinding process. The transformation of the chip formation mechanism and the shape of the chips during the grinding process of nickel-based superalloy GH4169 were first investigated. In addition, the effect of single grain grinding speed on chip morphology and chip formation frequency was analyzed. Finally, the reasonableness and accuracy of the simulation results are verified through experiments.

2 Experimental research

2.1 Experimental equipment

As shown in Fig.1, the grinding machine used in this paper is the M7120A, which processes workpieces with a maximum size of 630 × 200 × 320mm. The table uses a hydraulic system with step-less speed regulation. Because the surface grinding machine's spindle speed is constant, a Proton BT500 intelligent vector universal frequency converter is utilized to regulate the spindle speed to explore the impact of the grinding wheel's linear speed on the chip formation. The grinding wheel diameter is 180 mm and the abrasive chosen is CBN abrasive with the code 80/100 (average grain size of 180 μm) and medium hardness.

The inspection equipment consists of the LEXT OLS4100 3D measuring laser microscope, the Micromeasure 3D profiler and the Ultra Plus field emission scanning electron microscope (FEM). Where, the 3D measuring laser microscope mainly observes the surface profile and surface roughness of nickel-based superalloys, the 3D profiler for checking the three-dimensional profile of grinding surfaces, and the FEM is used to observe the metallographic organization and the shape of the grinding chips.

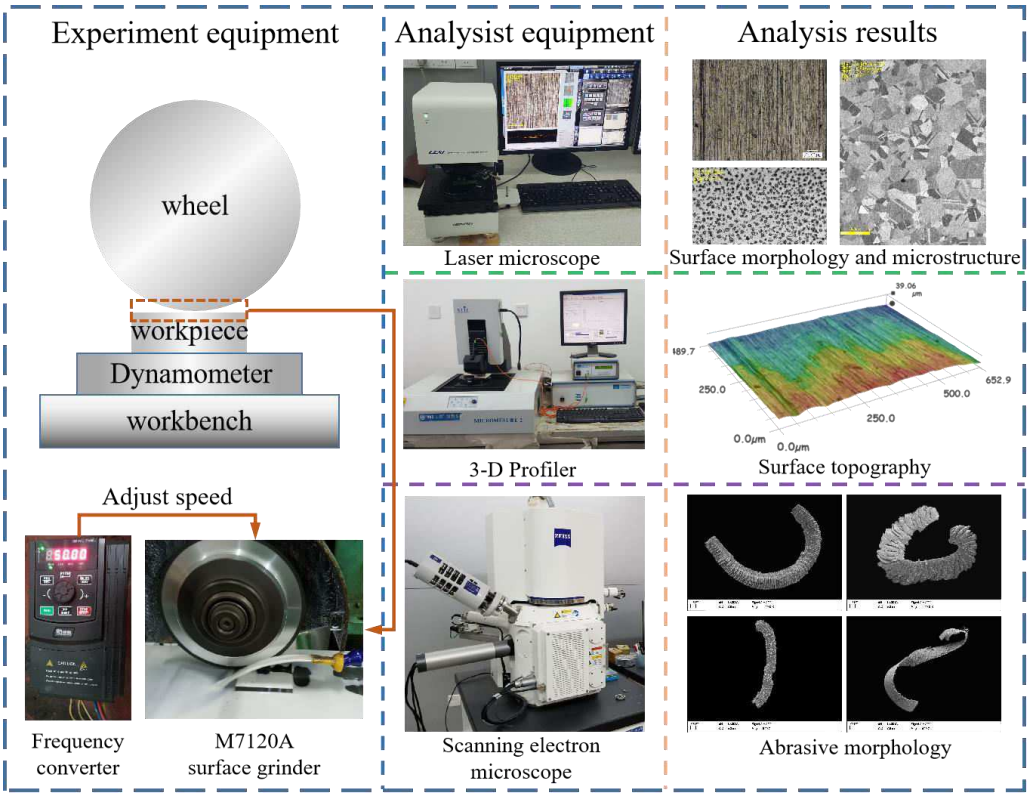

Fig.1 Experimental and analysis equipment for this paper

2.2 Experimental material

GH4169 is a precipitation-reinforced nickel-based superalloy with good fatigue, radiation, oxidation and corrosion resistance properties and is capable of producing a variety of complex-shaped components, which are widely used in aerospace, nuclear and petroleum industries as well as in extrusion dies. The microstructure of the nickel-based polycrystalline superalloy GH4169 was observed by field emission scanning electron microscopy, as shown in Fig.2, where the presence of many grains of varying sizes and the δ phase with an orthogonal ordered structure in the matrix of GH4169 can be significantly observed.

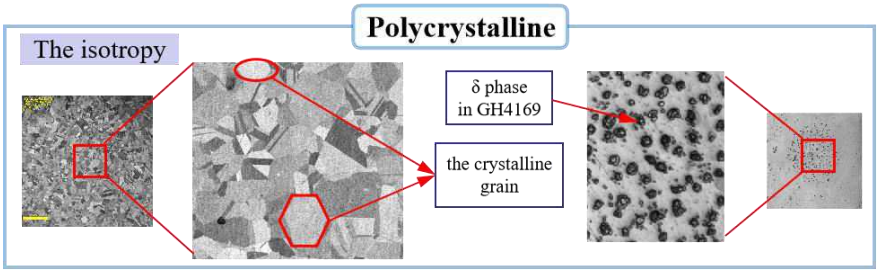

Fig.2 Microstructure of the nickel-based superalloy GH4169

3 Simulation

3.1 Modelling of abrasive and workpiece material

Although CBN grinding wheels have high hardness, good self-sharpening and high toughness, the shape of CBN abrasive grains varies significantly from one another, resulting in unrepresentative modeling of single

abrasive. Diamond abrasive grains not only have high wear resistance but also have a simpler shape, so single abrasive finite element simulation tests are often carried out using diamond abrasive. The simulated workpiece is the nickel-based superalloy GH4169, whose material properties are shown in Table 1.

Table 1 Selected material properties of diamond grain and GH4169

Material	E/(Gpa)	M	ρ/(kg/m^3)
Diamond	882	0.2	3523
GH4169	220	0.3	8240

A material's constitutive model represents the stress-strain-time relationship during the deformation of the material, and the selection of a correct and appropriate constitutive model can help improve the accuracy of the simulation. The Johnson-Cook constitutive equation takes into account the mechanical behavior of the metal under stress, strain, and temperature. It is suitable for describing the deformation behavior of nickel-based superalloys in the grinding environment. The Johnson-Cook model can be written as follows:

$$\sigma = (A + B\varepsilon^n)\left(1 + ln\frac{\dot{\varepsilon}}{\dot{\varepsilon}_0}\right)\left(1 - \left(\frac{T - T_{room}}{T_{melt} - T_{room}}\right)^m\right) \tag{1}$$

This equation consists of three parts: The first section depicts the strain effect on flow stress. The influence of strain rate on flow stress is illustrated in the second portion. And the third part represents the effect of temperature on flow stress. Where A means the initial yield stress; B represents the strain hardening constant; C indicates the strain rate strengthening factor; m denotes the thermal softening factor, and n is the hardening index; $\dot{\varepsilon}$ is the equivalent plastic strain rate; ε indicates the equivalent plastic strain; T denotes the workpiece deformation temperature; T_{melt} represents the material melting temperature and T_{room} is the room temperature. Where the specific values are shown in Table 2.

Table 2 Johnson-Cook model parameters of nickel-based superalloy GH4169

A/(Mpa)	B/(Mpa)	C	m	N	T_{melt}	T_{room}
1241	622	0.0134	1.3	0.6522	1300	25

The chip separation criterion is used in finite element calculations to determine whether or not the chips are separated from the material matrix at the front of the abrasive grain. An accurate separation criterion can truly reflect the material's physical properties and help to obtain reasonable results. Taking into account the stress and strain during the actual grinding process and the influence of temperature on the material, the Johnson-Cook damage model was chosen for the simulation, with fracture occurring when D exceeds 1. Where the Johnson-Cook damage model can be expressed as:

$$D = \sum\left(\frac{\Delta\bar{\varepsilon}^{pl}}{\bar{\varepsilon}_f^{pl}}\right) \tag{2}$$

Where $\Delta\bar{\varepsilon}^{pl}$ denotes the equivalent plastic strain increment; $\bar{\varepsilon}_f^{pl}$ is the failure strain.

Failure strain $\bar{\varepsilon}_f{}^{pl}$ can be expressed as:

$$\bar{\varepsilon}_f^{pl}=\left[D_1+D_2\exp\left(D_3\sigma^*\right)\right]\left(1+D_4\ln\dot{\bar{\varepsilon}}_0{}^*\right)\left(1+D_5T^*\right) \tag{3}$$

Where D_1, D_2, D_3, D_4, and D_5 are damage parameters with the specific values shown in Table 3. σ^* is the dimensionless partial compressive stress rate, in which $\sigma^*=\frac{p}{q}$ (p is the compressive stress and q is Mies stress); $\dot{\bar{\varepsilon}}_0{}^*=\frac{\dot{\bar{\varepsilon}}^{pl}}{\dot{\varepsilon}_0}$, $\dot{\bar{\varepsilon}}^{pl}$ is the failure strain rate, and $\dot{\varepsilon}_0$ is the reference failure strain rate; T^* is the dimensionless temperature, in which $T^*=\frac{T-T_0}{T_{melt}-T_0}$.

Table 3 Johnson-Cook shear failure parameters of nickel-based superalloy GH4169

Material	D_1	D_2	D_3	D_4	D_5
GH4169	-0.239	0.456	0.3	0.07	2.5

The friction model uses the modified Coulomb's law of friction:

$$\begin{cases}\tau_f=\mu\sigma_n,(\mu\sigma_n<\tau_s)\\ \tau_f=\tau_s,(\mu\sigma_n<\tau_s)\end{cases} \tag{4}$$

Where τ_f is the frictional force on the blade surface in front of the abrasive grain; μ represents the friction coefficient; σ_n denotes the positive stress; τ_s is the shear stress.

3.2 Three-dimensional finite element simulation model

3.2.1 Finite element models of the workpiece

As shown in Fig.3, The grinding thickness during single grain grinding varies with time. The grinding process first gradually increases from 0μm to the maximum undeformed cutting thickness a_{gmax} and then rapidly decreases to 0μm. The entire cutting area is curved in a wedge shape, and this model is difficult to build and is computationally intensive. Therefore, the workpiece model is simplified to a triangular structure to simplify the finite element model and increase the computational speed of the model.

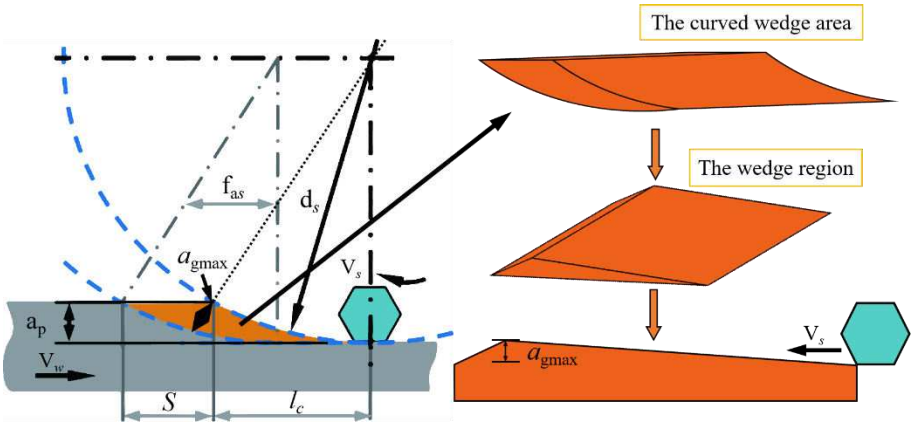

Fig.3 Finite element models of the workpiece

The a_{gmax} could be calculated by:

$$a_{\mathrm{gmax}} = 2\lambda_s \left(\frac{v_w}{v_s}\right) \sqrt{\frac{a_p}{d_{eq}}} \tag{5}$$

Where, a_{gmax} denotes the maximum undeformed cutting thickness; λ_s is the circumference of the grinding wheel; v_w represents the workpiece feed rate; v_s denotes the grinding wheel linear speed; a_p is the grinding depth; d_{eq} indicates the grinding wheel diameter (taken as 180 mm).

3.2.2 Finite element models of abrasive

Diamond abrasive grains not only have high wear resistance but also have a simple shape. So, the diamond abrasive was used in the simulation. The shape of the diamond abrasive and the simulation model are shown in Fig.4. A cutting surface of the diamond abrasive is chosen as the front face of the tool, with the cutting edge width of a and the cutting angle of 60°. The whole model is simplified to an octahedron with an isosceles trapezoid in the main view and a rectangle in the left view.

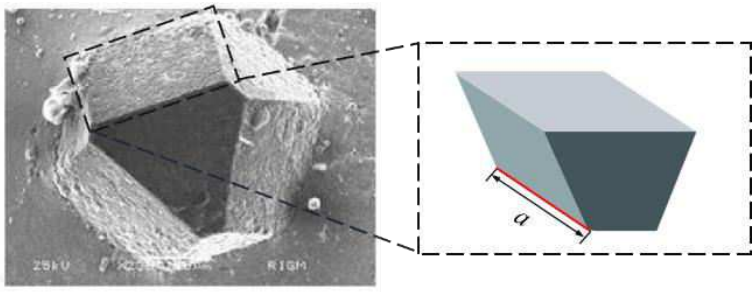

Fig.4 Finite element models of abrasive

3.3 Finite element simulation parameter setting for single abrasive

Fig.5 shows a simulation model of single abrasive grinding with a workpiece size of 60 μm, a width of 16 μm, and an a_{gmax} of 1.5 μm. As diamond is much harder than nickel-based superalloy GH4169, deformation and wear during grinding can be neglected, which is defined as a rigid body. The number of workpiece grid cells in Fig.5b is 2,122,720 and the number of tool cells is 126,968.

(a) Schematic diagram of the simulation grinding

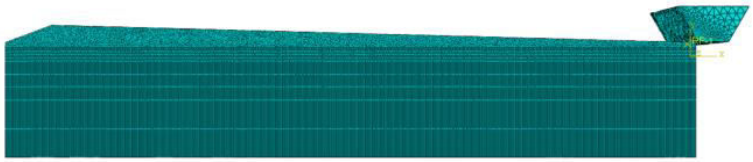

(b) Finite element model

Fig.5 Finite element simulation model of a single abrasive

The specific grinding parameters for the finite element simulation model are shown in Table 4 below:

Table 4 Grinding parameters applied in the finite element simulation model

Grinding speed/(m/s)	Feed rate/(m/min)	Grinding depth/(um)	Maximum undeformed cutting thickness /(um)
20	0.1688	40	1.5
25	0.2110		
30	0.2532		
35	0.2954		
45	0.3798		
60	0.5064		

4 Results and analysis

4.1 Surface profile analysis for grinding

Under the conditions of grinding speed v_s=35m/s, grinding thickness a_p=40μm and feed rate v_w=0.2954m/min, the grinding surface profile of nickel-based polycrystalline superalloy GH4169 and the simulated surface profile of a single abrasive were obtained as shown in Fig.6.

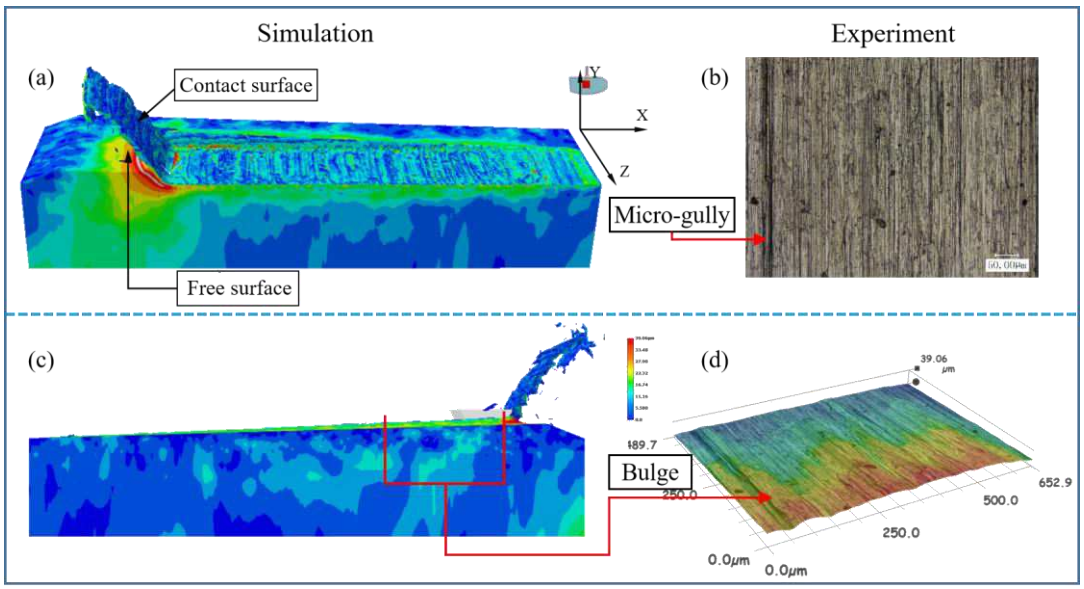

Fig.6 The surface morphology in grinding GH4169

Fig.6a shows the surface morphology of nickel-based superalloy GH4169 in single abrasive simulation, and Fig.6c shows a rear view of its XY surface, in which it can be clearly observed that the workpiece material undergoes plastic flow under the action of the abrasive, forming bulge on the front tool face and sides of the abrasive grain.

The surface morphology of the nickel-based polycrystalline superalloy GH4169 was observed under the same parameters. The surface morphology also showed bulges and micro-grooves (as shown in Fig.4b and Fig.4d). The reason for this is the deformation of the material under the action of the abrasive grains. When the force exceeds the elastic limit of the material, the material undergoes plastic flow and part of the material builds up under the action of the front face of the cutting edge and eventually forms a chip, while the other part of the material undergoes plastic flow to both sides to form a bulge or flying edge, which should be suppressed during the grinding process.

4.2 The chip morphology

To visualize the change in chip morphology during the grinding process, the grinding abrasive was concealed and the chip morphology of single abrasive grinding a nickel-based polycrystalline superalloy GH4169 was obtained, as shown in Fig.7a. And to verify the accuracy of the chip morphology during the simulation, a chip collecting box was installed on the grinding machine table to collect the chips generated during the grinding test, and the surface morphology was studied using the Ultra Plus field emission scanning electron microscope to get Fig.7b.

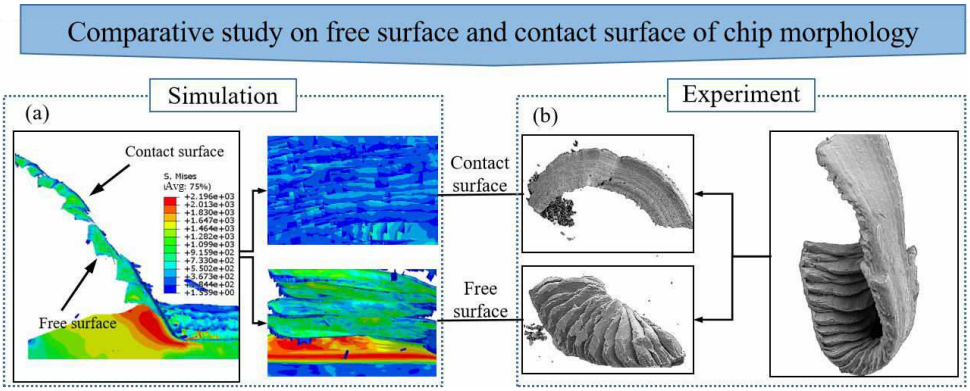

Fig.7 The free surface and contact surface of the chip

As shown in Fig.7a, nickel-based polycrystalline superalloy GH4169 mainly produces serrated chips during grinding, which have two distinct surfaces: the contact surface and the free surface. The side that is biassed towards the front face of the abrasive grain is called the contact surface, which is mainly smooth and flat and has traces of abrasive grains sliding over the inner surface of the abrasive chip. Its outflow direction is basically the same as the angle of the abrasive grain, while the bulge on the side of the abrasive grain also forms burrs and flying edges. The other side is called the free surface. Compared with the contact surface, the free surface is mainly manifested as a lamellar shape. The reason for this is that when the stress on the shear surface exceeds the strength limit of the material in the process of shaping and deforming the material under the action of the abrasive, the material is sheared to form lamellar nodules. Fig.7b shows the shape of the chips collected at the same grinding parameters, in which the free surface and the contact surface of the chips can be clearly observed, and the shape is similar to the simulation results.

During the machining process, the interaction between the abrasive and the workpiece generates a large amount of grinding heat. At the same time, the abrasive grain generally has a negative front angle. Thus, the grinding will intensify the material deformation and generate high temperatures. As a large amount of grinding heat is not released in time, it makes the material more susceptible to adiabatic shearing and the formation of jagged abrasive chips, the formation principle diagram of which is shown in Fig.8a.

Nickel-based superalloys have high strength, thermal strength and low thermal conductivity and are typically difficult-to-machine materials, so the grinding temperature generated during the grinding process is difficult to conduct out and the degree of adiabatic shear is more pronounced, making it easy for the shear slip to occur. Fig.8b shows the single abrasive simulation of nickel-based superalloy GH4169. In this picture, the jagged lamellar abrasive chips are visible, and there are clear bulges in the shear surface of the chip.

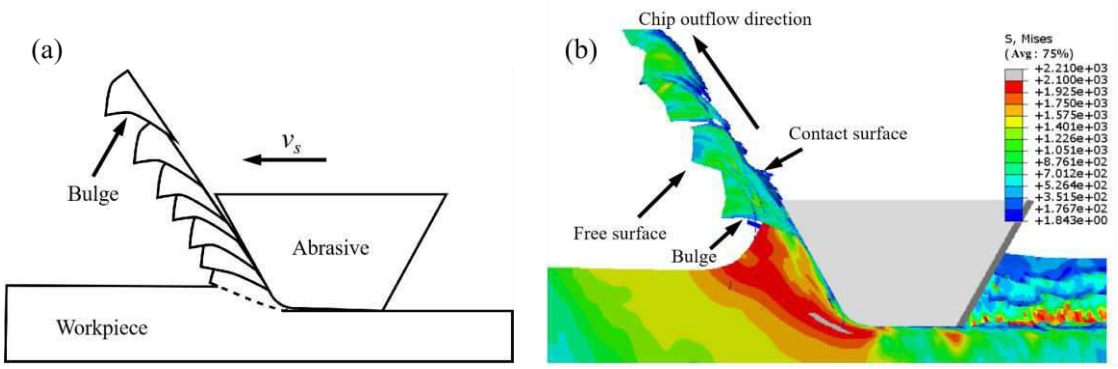

Fig. 8 Morphology of lamellar abrasive chips with serrated flakes

To explore the process of serrated abrasive chip formation, six images (Fig.9 a-b) were selected which correspond to the formation of chip in the previous section, material bulge, material fracture, material shear slip, material being squeezed to form a bulge, and the formation of the chip. As shown in Fig.9, the swarf gradually thickens during the grinding process, and when the swarf thickness reaches a certain value it cracks and quickly thins out. The formation of chips repeats the process periodically. This is because during the grinding process, the shear angle of the cutting edge decreases and the thickness of the grinding chip increases, resulting in more tremendous stress on the chip, when this stress reaches the fracture limit of the material, the material fractures, at which point the back draft decreases and the shear angle increases. In addition, it can be observed that a bulge is generated near the center of the shear surface of the abrasive chip. This is because, in the process of chip formation, the material does not only undergo sheer slip, the center of the shear surface of the abrasive chip is also squeezed to form a bulge.

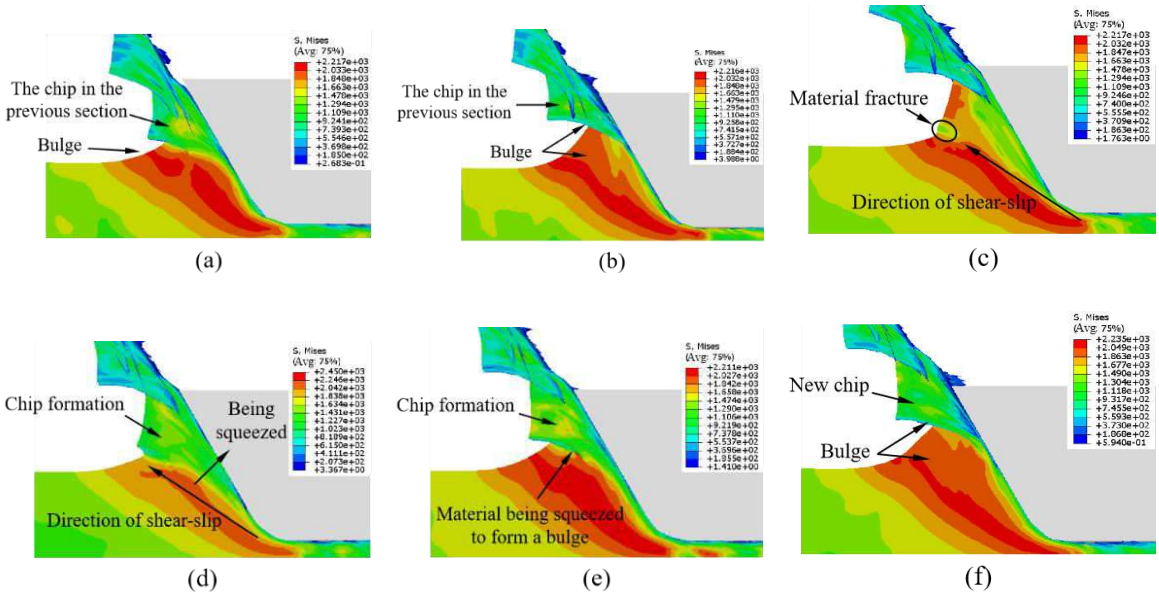

Fig.9 The process of abrasive chip formation

4.2.1 Influence of variation in cut thickness of single abrasive on chip morphology

At the maximum undeformed chip thickness of 1.5 μm and the single abrasive grinding speed of 35 m/s, the change in chip morphology with cutting thickness is shown in Fig.10.

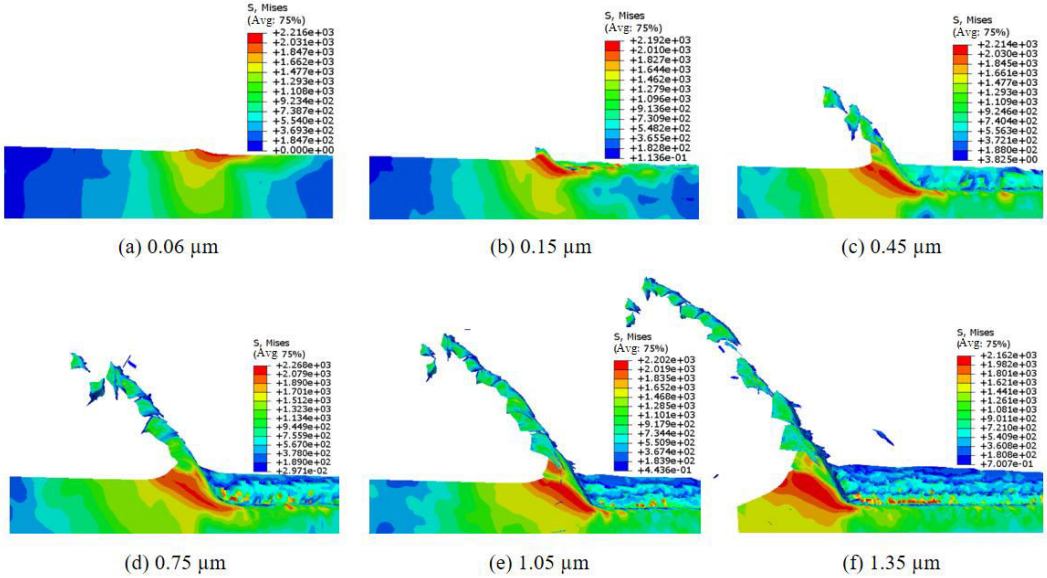

Fig.10 Variation of grinding morphology with the grinding process

When the cutting thickness of single abrasive is 0.06μm, the workpiece material forms a slight bulge at the front of the abrasive, and no chips are formed at this time. Then, at the cutting thickness of 0.15μm, the material deforms plastically and builds up in front of the abrasive grain, increasing the bulge and producing a small number of abrasive chips. By 0.45μm, the abrasive chips begin to increase but are mostly crumbly and unstable. At 0.75μm, the chip formation frequency rises and begins to stabilize, but the sawtooth shape of the chips is not significant. However, the sawtooth shape chips can be clearly observed from 1.05μm to 1.35μm and are more serrated at 1.35μm compared to those at 1.05μm. Therefore, the workpiece material undergoes four successive stages of grinding: rubbing - ploughing - unstable chip formation - stable chip formation. The material is deformed elastically by the force when the abrasive grain starts to come into contact with the workpiece. Subsequently, as the chip thickness of a single abrasive grain increases. When the force of the abrasive grain on the workpiece is greater than the elastic limit of the material, the workpiece material will be plastically deformed, thus causing the plastic flow of material to both sides of the cutting edge or the front tool face to form a bulge.

To further explore the variation of the workpiece material and abrasive interaction mechanism in the three stages of rubbing - ploughing - cutting, the stress diagrams of the three stages were retrieved from the simulation results, as shown in Fig.11. When the thickness of single abrasive is less than 0.06 μm, the interaction between the abrasive and the workpiece is small, with the maximum von Mises stress of only 2.216 GPa. At the same time, the workpiece material only undergoes elastic deformation, resulting in the abrasive cutting through the workpiece and not producing chips, as shown in Fig.11a. When the cutting depth is about 0.06μm to 0.18μm, the force between the abrasive grain and the workpiece will exceed the material's elastic limit, with the maximum von Mises stress of 2.328GPa. At the same time, the surface of the workpiece is plastically deformed, resulting in plastic flow and the formation of a bulge, as shown in Fig.11b. When the grinding depth continues to increase beyond 0.18μm, at which point the maximum von Mises stress reaches 2.791GPa, the material will tear down from the surface of the base material and begin to form chips, as shown in Fig.11c.

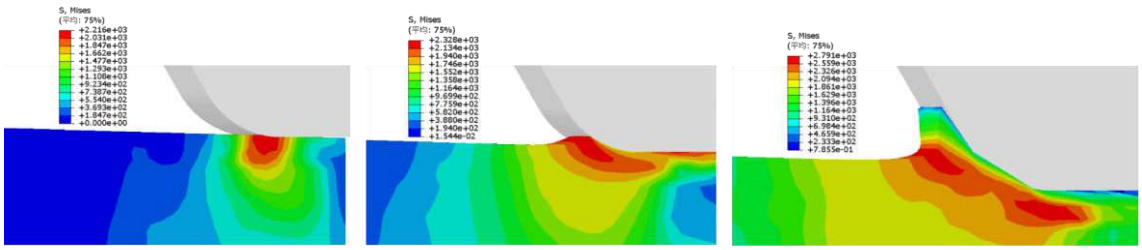

Fig.11 Processes of change in the mechanism of interaction between abrasive and material

During the grinding process, the grinding force oscillates at a high frequency in a violent cyclic manner, and each fluctuating cycle of the grinding force corresponds to the formation of a chip. The grinding force increases rapidly at the beginning of chip formation, decreases sharply after chip formation, and then increases when new chips are generated, a process that repeats itself. And the correctness of this theory has also been verified by the researchers involved [26, 28, 30]. To further explore the effect of the variation of the cutting thickness of a single abrasive on the chip formation stage, the values of the grinding force variation throughout the grinding process were retrieved, as shown in Fig.12.

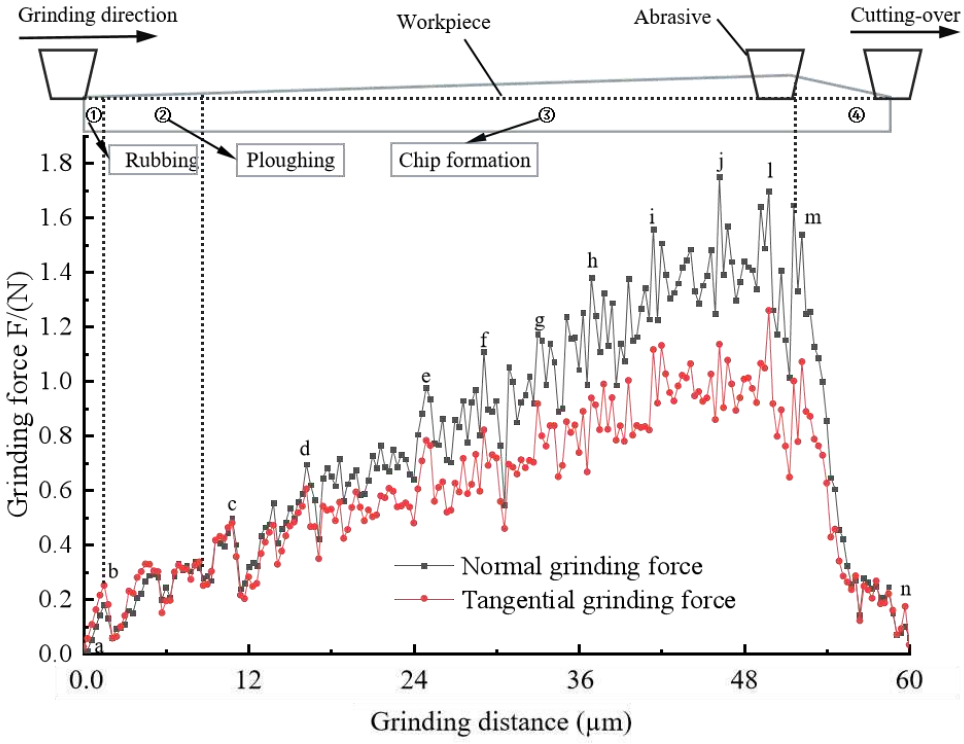

Fig.12 Variation of grinding forces during the grinding process of a single abrasive

In Fig.12, ①, ②, and ③ correspond to the three stages of the grinding process: rubbing, ploughing and chip formation. As the grinding distance increases and the depth of cut changes, the peak grinding forces show a gradual increase followed by a sharp decrease. The peak grinding force gradually increases from 0 N to 1.8 N when the cutting thickness of a single abrasive gradually increases to the maximum cutting thickness a_{gmax}. Subsequently, the peak grinding force also drops sharply to 0 N due to the sharp reduction in the cutting thickness of the single abrasive. Specifically, when grinding is in the rubbing stage, the constant squeezing of the abrasive results in a

linear increase in grinding force to 0.28 N. When grinding is in the ploughing stage, a slight bulge is produced on the front face of the grinding abrasive. However, there is no cyclicality in the change of grinding forces. When grinding is in the chip formation stage, it can be clearly observed that during the pre-chip formation, the chip segmentation frequency is unstable and the grinding forces are not cyclical. While after point e, it enters a stable chip formation state and the grinding force shows a cyclical increase.

Since the chip is in a stable chip state after point e, to quantitatively analyze the change in chip formation frequency during grinding, a total of 7 points from e-l are intercepted as data for calculating the chip formation frequency, where the chip segmentation frequency is the reciprocal of time. Fig.13a shows the change in chip segmentation frequency during single abrasive grinding.

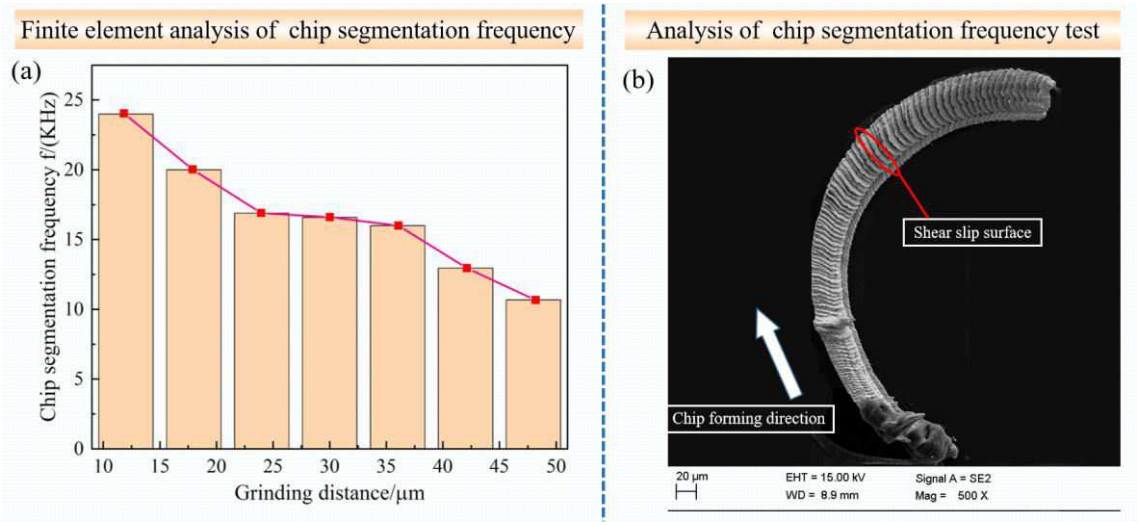

Fig.13 Change in chip segmentation frequency during single abrasive grinding

As shown in Fig.13a, the chip segmentation frequency of GH4169 gradually decreases with the increase of the cutting thickness of a single grinding abrasive. In particular, the chip segmentation frequency decreases sharply from 24 kHz to 20 kHz at grinding distances between 10μm and 24μm; at grinding distances between 24μm and 36μm, the chip segmentation frequency changes more slowly; at grinding distances between 36μm and 46μm, the chip segmentation frequency decreases sharply from 16 kHz to 11 kHz. Fig.13b shows the chip morphology observed by SEM in the grinding test. When chip formation begins, the chip shear slip surface is narrower and jagged units are formed more frequently because of the low chip depth. However, as the thickness of the cut increases, the width of the shear slip surface of the chip increases and the frequency of formation of serrated units on its free surface decreases. The results are the same as for the single grain simulation.

4.2.2 Influence of grinding speed on chip morphology

To explore the variation of chip morphology at different speeds, the chip morphology was observed at grinding speeds v_s= 20m/s, 25m/s, 30m/s, 35m/s, 40m/s and 60m/s respectively. The maximum cutting thickness of the single abrasive is 1.5μm and the grinding distance is 51μm. The finite element simulation results are shown in Fig.14A. Fig.14B shows the grinding chips collected under the same experimental parameters, and the grinding chip morphology was observed by scanning electron microscopy.

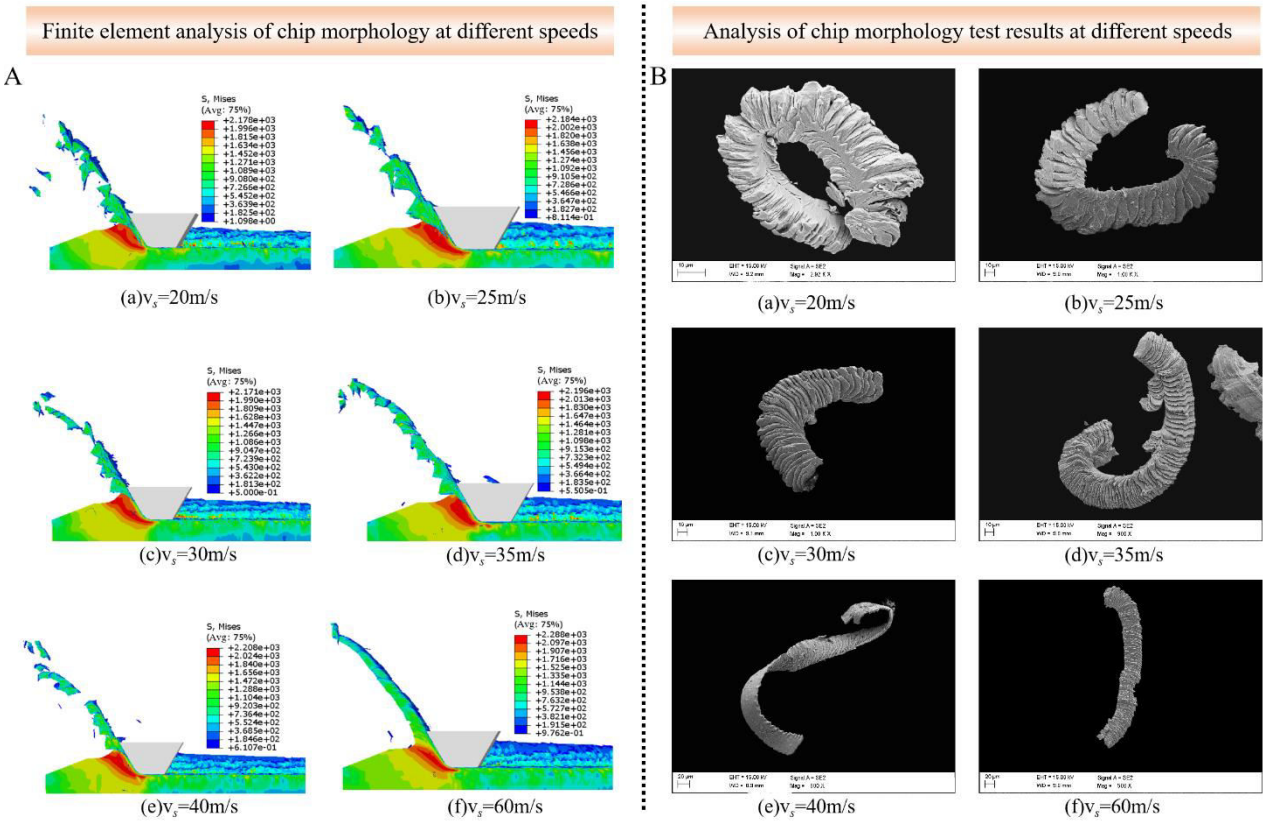

Fig.14 Chip morphology at different speeds

As shown in Fig.14A, the chip morphology in this grinding speed range is mainly in the form of serrated flakes, the free surface is serrated and the contact surface is smooth due to the extrusion of the abrasive. Generally speaking, as the grinding speed increases, the chip shape changes from a unitary laminated serrated chip to a continuous serrated chip, which then develops into a continuous ribbon chip. When the grinding speed is between 20m/s and 30m/s, the chip pattern is unitary lamellar serrated; At 35m/s to 40m/s, the chip pattern is continuous and serrated. At 35m/s to 40m/s, the chip pattern is continuous and serrated. At a grinding speed of 60 m/s, the chip pattern is a continuous strip, but the free surface of the chip still has a fine flaky layer. The reason for this is that GH4169 has a significant strain rate effect in this grinding speed range. When the grinding speed is small, the material strain hardening effect has a more significant influence on the material stresses, resulting in higher flow stresses and material hardness in the first deformation region than in other areas. Thus, under the action of the abrasive grain, the material in the first deformation zone forms a bump on the unmachined surface in the direction of shear, followed by a lamellar, serrated abrasive chip along the front face of the abrasive grain. As the grinding speed increases, the material hardening effect on the material stress gradually decreases, its shaping index decreases and it is easier to form continuous or banded chips.

As shown in Fig.14B, The chip morphology is mainly serrated at different grinding speeds, and the free surface and contact surface morphology are consistent with the morphology obtained from the simulation. In addition, it can be observed that when the grinding wheel line speed is 20m/s and 25m/s, the shear slip surface of the chip is wider and the frequency of segmentation of serrated units on its free surface and the degree of serration are lower. However, as the wheel line speed increases and when the wheel line speed is 30m/s to 60m/s, the shear slip surface becomes narrower, and the frequency of segmentation of serrated units on its free surface and the

degree of serration increases. The reason for this is that as the grinding speed increases, the rate of material deformation increases, material plasticity decreases, and toughness increases, making it easier to form abrasive chips and shear slip occurs more frequently.

The above method of calculating the chip formation frequency for the stable chip formation phase gives the stable chip formation frequency at different speeds, as shown in Fig.15.

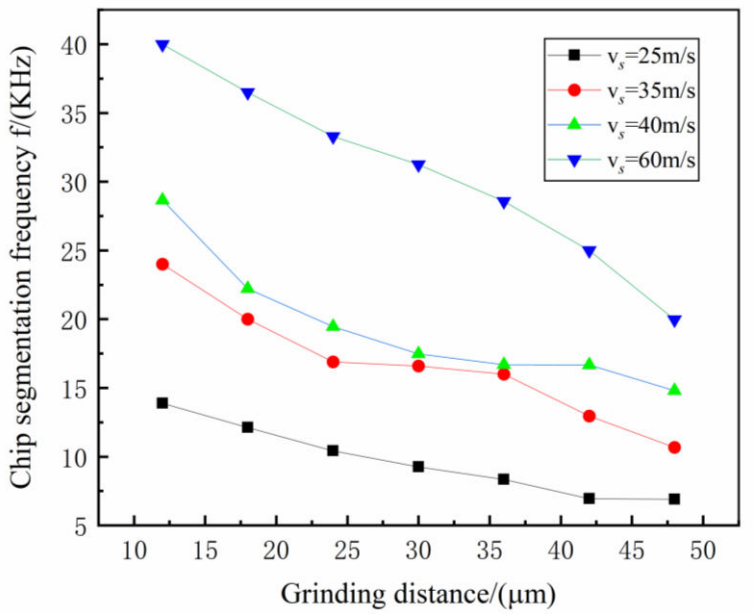

Fig.15 Influence of the cutting thickness of the single abrasive on the frequency of chip segmentation at different grinding speeds

It can be observed from Fig.15 that the chip segmentation frequency of GH4169 decreases with the increase of grinding distance in the range of simulation parameters and increases from 14 kHz to 40 kHz with the addition of grinding speed (25 m/s~60 m/s) when the grinding distance is the same. The trend of the chip segmentation frequency was consistent with the test results, which confirmed the reliability of the model establishment.

5 Conclusions

In this paper, the mechanism of chip formation in the grinding process of nickel-based superalloy GH4169 was investigated. By establishing a 3-dimensional finite element model of grinding based on the actual variation of the cutting thickness of a single abrasive grain, the variation of chip morphology during grinding process and the effect of grinding speed on chip morphology were analyzed. At the same time, the simulation results were also verified by collecting grinding chips with the same grinding parameters. The following results were obtained in this study.

1. The nickel-based polycrystalline superalloy GH4169 mainly generates serrated chips during the grinding process, which has two typical surfaces: the contact surface and the free surface. The grinding force varies cyclically and its fluctuations correspond to the chip formation process.

2. The grinding process can be divided into four stages according to the change in the mechanism of action between the abrasive and the material: rubbing, ploughing, unstable chip formation and stable chip formation. The frequency of chip segmentation decreases as the grinding distance increases, mainly attributed to the increase in the

cutting thickness of the single abrasive grain. In addition, the grinding speed is also a significant factor affecting the frequency of chip formation in grinding. Specifically, the higher the grinding speed, the higher the frequency of chip segmentation in grinding.

3. As the grinding speed increases, the chip morphology changes from a lamellar chip to a continuous chip pattern, and then develops into a continuous band of chips. At a grinding speed of 20m/s to 30m/s, the chip pattern becomes a unitary lamellar chip; at a grinding speed of 35m/s to 40m/s, the chip pattern becomes a continuous serrated chip; at a grinding speed of 60m/s, the chip pattern becomes a continuous ribbon chip, but the free surface of the chip still has a fine lamellar layer.

Reference

1. Li S, Wu Y, Nomura M (2016) Effect of grinding wheel ultrasonic vibration on chip formation in surface grinding of Inconel 718. Int J Adv Manuf Technol 86, 1113–1125. https://doi.org/10.1007/s00170-015-8149-0.

2. Gong Y, Zhou Y, Wen X, et al (2017) Experimental study on micro-grinding force and subsurface microstructure of nickel-based single crystal superalloy in micro grinding. J Mech Sci Technol 31, 3397–3410. https://doi.org/10.1007/s12206-017-0629-8.

3. Zhou YG, Gong YD, Zhu ZX, Gao Q, Wen X (2016) Modelling and optimization of surface roughness from micro grinding of nickel-based single crystal superalloy using the response surface methodology and genetic algorithm. Int J Adv Manuf Technol, 85(9-12), 2607-2622. https://doi.org/10.1007/s00170-015-8121-z.

4. Gu YL, Nan LH, Du, B C, Ding W (2019) Towards the understanding of creep-feed deep grinding of dd6 nickel-based single-crystal superalloy. Int J Adv Manuf Technol, 100(2). https://doi.org/10.1007/s00170-018-2686-2.

5. Miao Q, Ding W, Kuang W, Yang C (2020) Comparison on grindability and surface integrity in creep feed grinding of gh4169, k403, dz408 and dd6 nickel-based superalloys. J Manuf Process, 49, 175-186. https://doi.org/10.1016/j.jmapro.2019.11.027.

6. Dai CW, Yu TY, Ding, WF, Xu JH, Yin Z, Li H (2019) Single diamond grain cutting-edges morphology effect on grinding mechanism of Inconel 718. Precis Eng, 55 119-126. https://doi.org/10.1016/j.precisioneng.2018.08.017.

7. Dai CW, Ding W F, Zhu YJ, Xu JH, Yu H W (2017) Grinding temperature and power consumption in high speed grinding of Inconel 718 nickel-based superalloy with vitrified CBN wheels. Precis Eng, S0141635917305627. https://doi.org/10.1016/j.precisioneng.2017.12.005.

8. Ming C, Yadong G, Yao S, Shuoshuo Q, Yin L, Yuying Y (2019) Experimental study on grinding surface properties of nickel-based single crystal superalloy dd5. Int J Adv Manuf Technol, 101. https://doi.org/10.1007/s00170-018-2839-3.

9. Ming C, Yadong G, Qu SS, Yang YY (2019) Experiment of Grinding Surface Quality and Subsurface Microstructure for Nickel-Based Single Crystal Superalloy. J Northeast Univ, 40(03):386-391. https://doi.org/10.12068/j.issn.1005-3026.2019.03.016.

10. Ding W, Dai C, Yu T, Xu J, Fu Y (2017) Grinding performance of textured monolayer CBN wheels: undeformed chip thickness nonuniformity modeling and ground surface topography prediction. Int J Mach Tools Manuf, 122, 66-80. https://doi.org/10.1016/j.ijmachtools.2017.05.006.

11. Ruzzi R, Paiva R, Silva L, Abro AM, Silva R (2021) Comprehensive study on Inconel 718 surface topography after grinding. Tribol Int, 158, 106919. https://doi.org/10.1016/j.triboint.2021.106919.

12. Li C, Piao YC, Meng BB, Hu YX, Li LQ, Zhang FH (2022). Phase transition and plastic deformation mechanisms induced by self-rotating grinding of GaN single crystals. Int J Mach Tools Manuf, 172. https://doi.org/10.1016/j.ijmachtools.2021.103827.

13. Öpöz TT, Chen X (2012) Experimental investigation of material removal mechanism in single grit grinding. Int J Mach Tools Manuf, 63, 32-40. https://doi.org/10.1016/j.ijmachtools.2012.07.010.

14. Öpöz TT, Chen X (2014) Experimental study on single grit grinding of Inconel 718. Procee Ins Mech Eng Part B J Eng Manuf, 229(5). https://doi.org/10.1177/0954405414531114.

15. Chen X, Öpöz TT (2013). Comparison of material removal characteristics in single and multiple cutting edge scratches. Adv Mat Res, 797, 189-195. https://doi.org/10.4028/www.scientific.net/AMR.797.189.

16. Zhao JY, Yu CF, Xu JH, Lin T, Lu Y (2013) Forces and chip morphology of nickel-based superalloy Inconel 718 during high speed grinding with single grain. Key Eng Mater, 589-590, 209-214. https://doi.org/10.4028/www.scientific.net/KEM.589-590.209.

17. Chen Z, Tian L, Fu Y, Xu J, Ding W, Su H (2012) Chip formation of nickel-based superalloy in high speed grinding with single diamond grit. Int J Abras Technol, 5(2), 93-106. https://doi.org/10.1504/IJAT.2012.048537.

18. Tian L, Fu Y, Xu J, Li H, Ding W (2015) The influence of speed on material removal mechanism in high speed grinding with single grit. Int J Mach Tools Manuf, 89, 192-201. https://doi.org/10.1016/j.ijmachtools.2014.11.010.

19. Feng BF, Cai GQ, Sun XL (2006) Groove, chip and force formation in single grain high-speed grinding. Key Eng Mater, 304-305, 196-200. https://doi.org/10.4028/www.scientific.net/KEM.304-305.196.

20. Ruzzi RDS, Silva RBD, Silva LRRD, Machado AR, Jackson MJ, Hassui A (2020) Influence of grinding parameters on Inconel 625 surface grinding. J Manuf Process, 55, 174-185. https://doi.org/10.1016/j.jmapro.2020.04.002.

21. Li B, Dai C, Ding W, Yang C, Shumyacher V (2020) Prediction on grinding force during grinding powder metallurgy nickel-based superalloy fgh96 with electroplated CBN abrasive wheel. Chinese J Aeronaut. https://doi.org/10.1016/j.cja.2020.05.002.

22. Denkena B, Köhler J, Kästner J (2012) Chip formation in grinding: an experimental study. Prod Eng Res Devel. 6, 107–115. https://doi.org/10.1007/s11740-011-0360-8.

23. Brinksmeier E, Aurich JC, Govekar E, Heinzel C, Hoffmeister HW, Klocke F, Peters J, Rentsch R, Stephenson DJ, Uhlmann E, Weinert K, Wittmann M (2006) Advances in Modeling and Simulation of Grinding Processes. CIRP Ann, 55(2), 667-696. https://doi.org/10.1016/j.cirp.2006.10.003.

24. Chen JB, Fang QH, Zhang LC (2014) Investigate on distribution and scatter of surface residual stress in ultra-high speed grinding. Int J Adv Manuf Technol, 75:615 – 627. https://doi.org/10.1007/s00170-014-6128-5.

25. Esmaeili H, Adibi H, Rezaei SM (2021) Study on surface integrity and material removal mechanism in eco-friendly grinding of Inconel 718 using numerical and experimental investigations. Int J Adv Manuf Technol, 112:1797 – 1818. https://doi.org/10.1007/s00170-020-06528-8.

26. Fu D, Ding W, Miao Q, Xu J (2017) Simulation research on the grinding forces and stresses distribution in single-grain surface grinding of ti-6al-4v alloy when considering the actual cutting-depth variation. Int J Adv Manuf Technol, 91:3591–3602.

https://doi.org/10.1007/s00170-017-0084-9.

27. Zhang C, Choi H (2021) Study of segmented chip formation in cutting of high-strength lightweight alloys. Int J Adv Manuf Technol, 112(9), 2683-2703. https://doi.org/10.1007/s00170-020-06057-4.

28. Dai J, Ding W, Zhang LC, Xu JH, Su HH (2015) Understanding the effects of grinding speed and undeformed chip thickness on the chip formation in high-speed grinding. Int J Adv Manuf Technol 81, 995–1005 (2015). https://doi.org/10.1007/s00170-015-7265-1.

29. Zhou W, Su H, Dai J, Yu T, Y Zheng (2018) Numerical investigation on the influence of cutting-edge radius and grinding wheel speed on chip formation in sic grinding. Ceram Int, 44, 21451-21460. https://doi.org/10.1016/j.ceramint.2018.08.206.

30. Xia J, Ding WF, Qiu B, Xu JH (2020) 3D simulation study on the chip formation process in high speed and ultra-high speed grinding of nickel-based superalloy. Diamond Abras Eng, 40(06):58-69. https://doi.org/10.13394/j.cnki.jgszz.2020.6.0011.

Statements and Declarations

Funding This work was supported by the National Natural Science Foundation of China (NO. U1908230&51775100), the Science and Technology Research Project of the Educational Department of Liaoning Province (NO. LJKZ0384), the Talent Scientific Research Fund of LNPU (NO. 2021XJJL-007).

Competing Interests The authors have no relevant financial or non-financial interests to disclose.

Author Contribution Tao Zhu: Writing - original draft, software, investigation, visualization. Ming Cai: Writing - original draft, review and editing, conceptualization, funding, visualization. Yadong Gong: Conceptualization, methodology, formal analysis. Xingjun Gao: Supervision, investigation, methodology. Ning Yu: Data curation, formal analysis. Xiang Li: Data curation, formal analysis.